PR-Set7–dependent lysine methylation ensures genome replication and stability through S phase

Mathieu Tardat,[1,2] Rabih Murr,[3] Zdenko Herceg,[3] Claude Sardet,[1,2] and Eric Julien[1,2]

[1]University of Montpellier II, Institut de Génétique Moléculaire de Montpellier, 34293 Montpellier, Cedex 5, France
[2]Centre National de la Recherche Scientifique, Unité Mixte de Recherche 5535, Institut Fédératif de Recherche 122, 34293 Montpellier, France
[3]International Agency for Research on Cancer, World Health Organization, 69372 Lyon, France

PR-Set7/SET8 is a histone H4–lysine 20 methyltransferase required for normal cell proliferation. However, the exact functions of this enzyme remain to be determined. In this study, we show that human PR-Set7 functions during S phase to regulate cellular proliferation. PR-Set7 associates with replication foci and maintains the bulk of H4-K20 mono- and trimethylation. Consistent with a function in chromosome dynamics during S phase, inhibition of PR-Set7 methyltransferase activity by small hairpin RNA causes a replicative stress characterized by alterations in replication fork velocity and origin firing. This stress is accompanied by massive induction of DNA strand breaks followed by a robust DNA damage response. The DNA damage response includes the activation of ataxia telangiectasia mutated and ataxia telangiectasia related kinase–mediated pathways, which, in turn, leads to p53-mediated growth arrest to avoid aberrant chromosome behavior after improper DNA replication. Collectively, these data indicate that PR-Set7–dependent lysine methylation during S phase is an essential post-translational mechanism that ensures genome replication and stability.

Introduction

To ensure the accurate inheritance of genetic information, cells must not only replicate their DNA but also duplicate the structure of chromatin and its higher order packaging during S phase of the cell cycle. Alteration of these processes can have devastating consequences leading to DNA damage and genomic instability, as observed in cancer cells (Venkitaraman, 2005). Whereas transmission of DNA methylation patterns can be easily explained by coupling enzymatic modification to the semiconservative DNA replication process (Leonhardt et al., 1992; Chuang et al., 1997), it is still unclear how the epigenetic marks and higher order structures of chromatin are maintained during DNA replication and faithfully transmitted.

PR-Set7 (also known as SET8) is a single polypeptide with an evolutionary conserved SET domain that specifically catalyzes monomethylation of histone H4-K20 (H4-K20me1; Fang et al., 2002; Nishioka et al., 2002; Couture et al., 2005; Xiao et al., 2005), whereas dimethylation (H4-K20me2) and trimethylation (H4-K20me3) of the same lysine are triggered by several other histone methyltransferases, including Suv420h1/2 (Schotta et al., 2004), NSD1 (Rayasam et al., 2003), and Ash1 (Beisel et al., 2002). H4-K20 trimethylation (H4-K20me3) selectively marks constitutive pericentromeric heterochromatin (Schotta et al., 2004) and imprinting control regions (Delaval et al., 2007), whereas mono- and dimethylation are broadly distributed but principally enriched in euchromatin regions (Nishioka et al., 2002; Karachentsev et al., 2005). Although the biological function of H4-K20me remains poorly understood, several studies have suggested that H4-K20me2 is involved in the guidance of DNA repair proteins to DNA strand breaks (Sanders et al., 2004; Botuyan et al., 2006), whereas H4-K20me1 is associated with chromatin condensation processes (Trojer et al., 2007). Furthermore, changes in H4-K20me3 patterns are frequently observed in human cancers (Fraga et al., 2005), suggesting that the epigenetic signal achieved with this methyl residue can affect important chromatin-templated processes with far-reaching consequences for normal and neoplastic development.

As part of the initial characterization of PR-Set7 functions, its levels in HeLa cells were found to be cell cycle regulated with a peak during M phase (Rice et al., 2002). Furthermore, PR-Set7 becomes phosphorylated at the G2/M transition (Georgi et al., 2002) and remains associated with chromosomes

Correspondence to Claude Sardet: claude.sardet@igmm.cnrs.fr; or Eric Julien: eric.julien@igmm.cnrs.fr

Abbreviations used in this paper: 7AAD, 7-amino-actinomycin D; ATM, ataxia telangiectasia mutated; ATR, ataxia telangiectasia related; CldU, chlorodeoxyuridine; HNF, human normal fibroblast; IdU, iododeoxyuridine; shRNA, small hairpin RNA.

The online version of this article contains supplemental material.

The Journal of Cell Biology, Vol. 179, No. 7, December 31, 2007 1413–1426
http://www.jcb.org/cgi/doi/10.1083/jcb.200706179

during mitosis (Rice et al., 2002). Collectively, these observations suggested that this enzyme might be involved in some aspects of cell division control. Consistent with this hypothesis, inactivation of the *Drosophila melanogaster* PR-Set7 orthologue causes defective mitotic progression and activation of DNA damage checkpoints in highly dividing cells of larval tissues, including imaginal disc cells and third instar larval neuroblasts (Karachentsev et al., 2005; Sakaguchi and Steward, 2007). Conversely, up-regulation of mammalian PR-Set7 expression upon loss of the transcriptional regulator HCF-1 leads to improper mitotic H4-K20 methylation levels and cytokinesis defects in HeLa cells (Julien and Herr, 2004). However, it remained unclear whether these mitotic defects were the effect of PR-Set7 functions in the mitotic process or whether they were the end point of cellular alterations generated before the onset of mitosis, thereby raising the question of PR-Set7 functions during the different phases of the cell cycle.

In this paper, we study the functions of human PR-Set7. Our results show that PR-Set7 regulates cell cycle progression by playing a key role during S phase. PR-Set7 associates with sites of DNA synthesis and regulates replication-fork progression. Inhibition of its catalytic activity causes improper DNA replication and loss of H4-K20 mono- and trimethylation. These defects are associated with massive induction of DNA breaks that leads to a p53-dependent DNA damage response to avoid entry into mitosis and aberrant chromosome behavior. Collectively, our results establish that PR-Set7–dependent lysine methylation is an essential posttranslational modification that contributes to genome replication and stability through S phase.

Results

PR-Set7 localizes with sites of DNA synthesis

As previously described by others in HeLa cells (Rice et al., 2002), we observed in both human osteosarcoma U2OS cells and human normal fibroblasts (HNFs) that PR-Set7 protein levels fluctuate during the cell cycle with a peak during M phase (Fig. S1 A, available at http://www.jcb.org/cgi/content/full/jcb.200706179/DC1). During G1 and S phases, PR-Set7 protein levels were low and almost undetectable using conventional immunostaining on fixed cells (Rice et al., 2002; and unpublished data). This is largely caused by a high turnover of the PR-Set7 proteins driven by a proteasome-dependent degradation process (unpublished data). Accordingly, short incubation (1 h) of U20S cells with the proteasome inhibitor MG132 rendered endogenous PR-Set7 easily detectable by immunofluorescence in all asynchronously growing cells, with ~35% showing a small, punctated nuclear staining (Fig. 1 A, left). Importantly, transient transfection of an HA epitope–tagged PR-Set7 in U2OS cells resulted in the same punctated pattern (Fig. S1 B), whereas it was not observed in cells depleted for PR-Set7 by siRNA treatment (not depicted). Because PR-Set7 has been described as a chromatin-associated protein, we checked whether these PR-Set7 foci colocalized with previously described chromatin/DNA foci (Baus et al., 2003; Peters et al., 2003). Strikingly, they did not colocalize with HP1 heterochromatin foci or with γ-H2A.X DNA damage foci after bleomycin treatment (Fig. 1 A, merged panels). In contrast, PR-Set7 foci colocalized with the sites of DNA synthesis detected by a short pulse (10 min) of BrdU incorporation (Fig. 1 B, merged panel). Accordingly, coimmunostaining was also detected with the proliferating nuclear antigen A and the DNA polymerase epsilon, two components of the replication machinery (Fig. 1 C, merged panels). This colocalization was observed at all stages of S phase based on the size and nuclear localization of BrdU-positive replication foci (unpublished data). Collectively, these results suggested that PR-Set7 might be important for DNA replication and S-phase progression.

PR-Set7–depleted cells display improper S-phase progression

To investigate whether PR-Set7 plays a role in DNA replication, we used a small hairpin RNA (shRNA)–expressing retroviral vector to stably express a PR-Set7 shRNA designed to silence PR-Set7 expression. Specificity of the PR-Set7 shRNA (shPR7) was verified by an shRNA-based protein replacement approach (Julien and Herr, 2003) in which an HA epitope–tagged PR-Set7 protein resistant to shPR7 treatment was expressed at physiological levels. As shown in Fig. 2 A, expression of the PR-Set7–specific shRNA (shPR7) but not of an irrelevant luciferase-specific shRNA (shLuc) led to the successful depletion of PR-Set7 2 d after cell infection, whereas the β-actin protein level was not affected (middle and bottom; compare lane 1 with lane 2). As expected, ectopic expression of the shRNA-resistant wild-type PR-Set7 protein was sufficient to rescue PR-Set7 expression in shPR7-expressing cells (Fig. 2 A, lanes 3 and 4). In the following experiments, we used these shRNA-resistant wild-type PR-Set7 protein U2OS cells ($U2OS_{SR}$) as a control to ascertain that the phenotype induced by shPR7 was specific of PR-Set7 depletion.

We first compared the proliferation rates of U2OS cells expressing either shLuc or shPR7 and $U2SO_{SR}$ cells expressing shPR7. As shown in Fig. 2 B, shPR7 U2OS cells displayed a marked decrease in cell proliferation soon after shRNA treatment. In contrast, shPR7 $U2OS_{SR}$ cells continued to proliferate at nearly the same rate as shLuc U2OS cells. We next analyzed the cell cycle profiles of the three cell lines at days 2, 3, and 4 after shRNA expression by measuring their DNA content. The results are shown in Fig. 2 C. In contrast to shLuc U2OS (Fig. 2 C; a, d, and g) and shPR7 $U2OS_{SR}$ cells (Fig. 2 C; c, f, and i), shPR7 U2OS cells (Fig. 2 C; b, e, and h) started to accumulate in S phase (from 26 to 56%) 3 d after shRNA expression. Importantly, a similar phenotype was also observed with normal and transformed human fibroblasts (see Fig. 5), suggesting that this result is not cell type specific. Furthermore, 24 h after the onset of the S-phase accumulation, a significant increase in the percentage of cells in the G2/M stage was detected (20 ± 8%), suggesting that some PR-Set7–depleted cells were still able to progress through and exit S phase, albeit slower than control cells (Fig. 2 C, day 4). Importantly, none of these cells were immunostained by an antibody against the mitotic marker phosphohistone H3 S10 (unpublished data), indicating that PR-Set7–depleted cells that had exited S phase were likely arrested in G2. Thus, consistent with its localization at sites of DNA synthesis (Fig. 1, A and C),

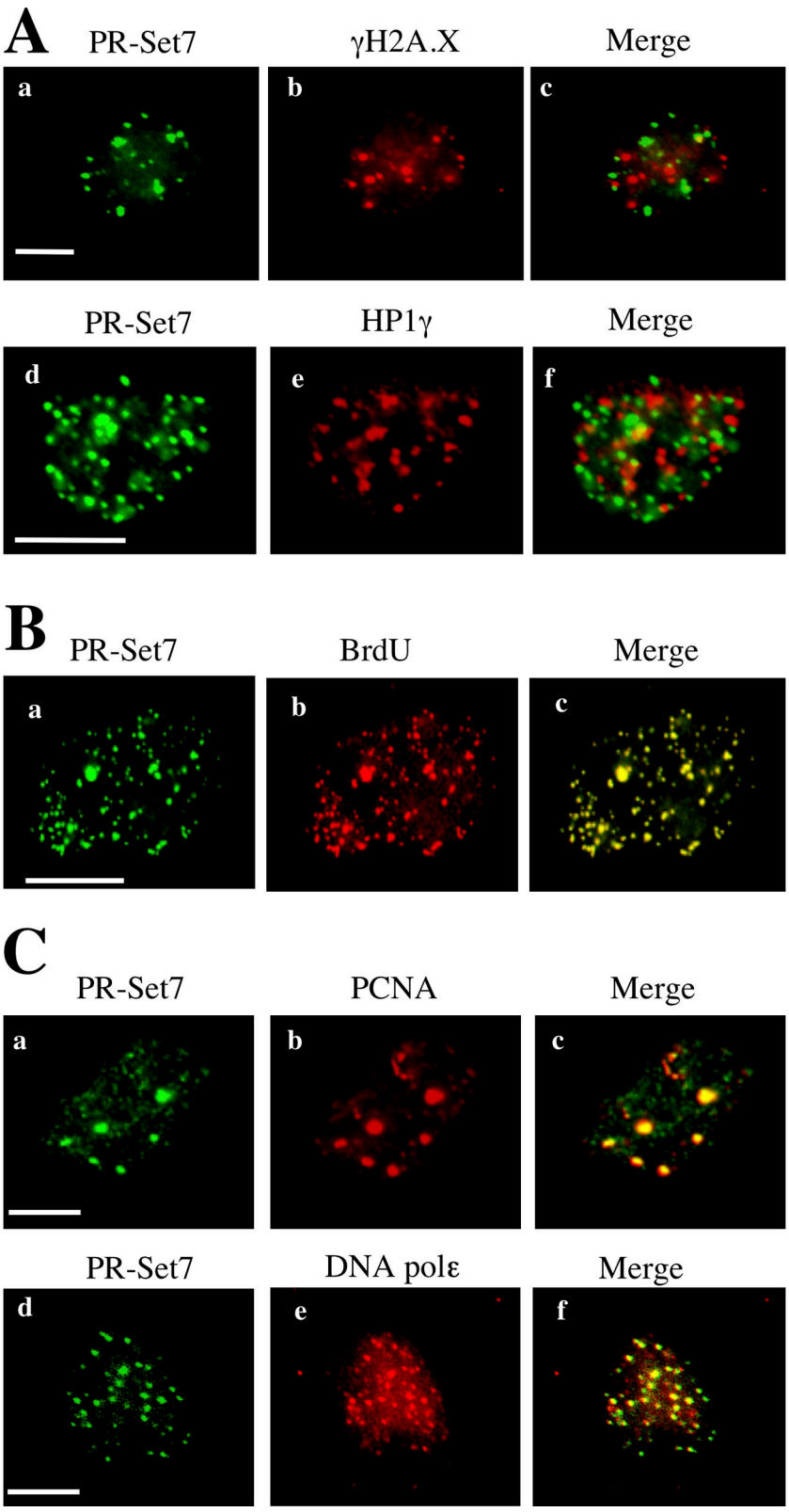

Figure 1. **PR-Set7 localizes at sites of DNA synthesis.** (A) Nuclei of asynchronously growing U2OS cells treated for 1 h with 15 μM MG132 to inhibit proteasome degradation and permeabilized for 10 min with 0.5% Triton X-100 to remove soluble nuclear and cytoplasmic proteins before PFA fixation. Cells were stained with anti–PR-Set7 (a and d), anti–γ-H2A.X (b), or anti-HP1γ (e) antibodies. Staining with anti–PR-Set7 (d) and anti–γ-H2A.X (b) was performed in U2OS cells treated with both MG132 and 25 μg/ml bleomycin for 1 h before fixation. (B) Nuclei of U2OS cells stained with anti–PR-Set7 (a) and anti-BrdU (b) antibodies. Cells were pulse labeled for 10 min with BrdU and treated as described in A before fixation. (C) Nuclei of asynchronously growing U2OS cells treated as described in A and stained with anti–PR-Set7 (a and d), anti–proliferating nuclear antigen A (b), or anti-DNA polymerase ε (e) antibodies. Bars, 5 μm.

PR-Set7 silencing leads to a defective S-phase progression in mammalian cells.

Other studies have shown that human PR-Set7 also associates with mitotic chromosomes (Rice et al., 2002), raising the possibility that PR-Set7 also plays a role during M phase of the cell cycle. To determine whether the improper S-phase progression of PR-Set7–depleted cells resulted from S-phase alterations or from alterations that occurred during the previous M phase, we synchronized U2OS and $U2OS_{SR}$ cells at the G1/S border 36 h after shRNA expression. At this time, shPR7 U2OS

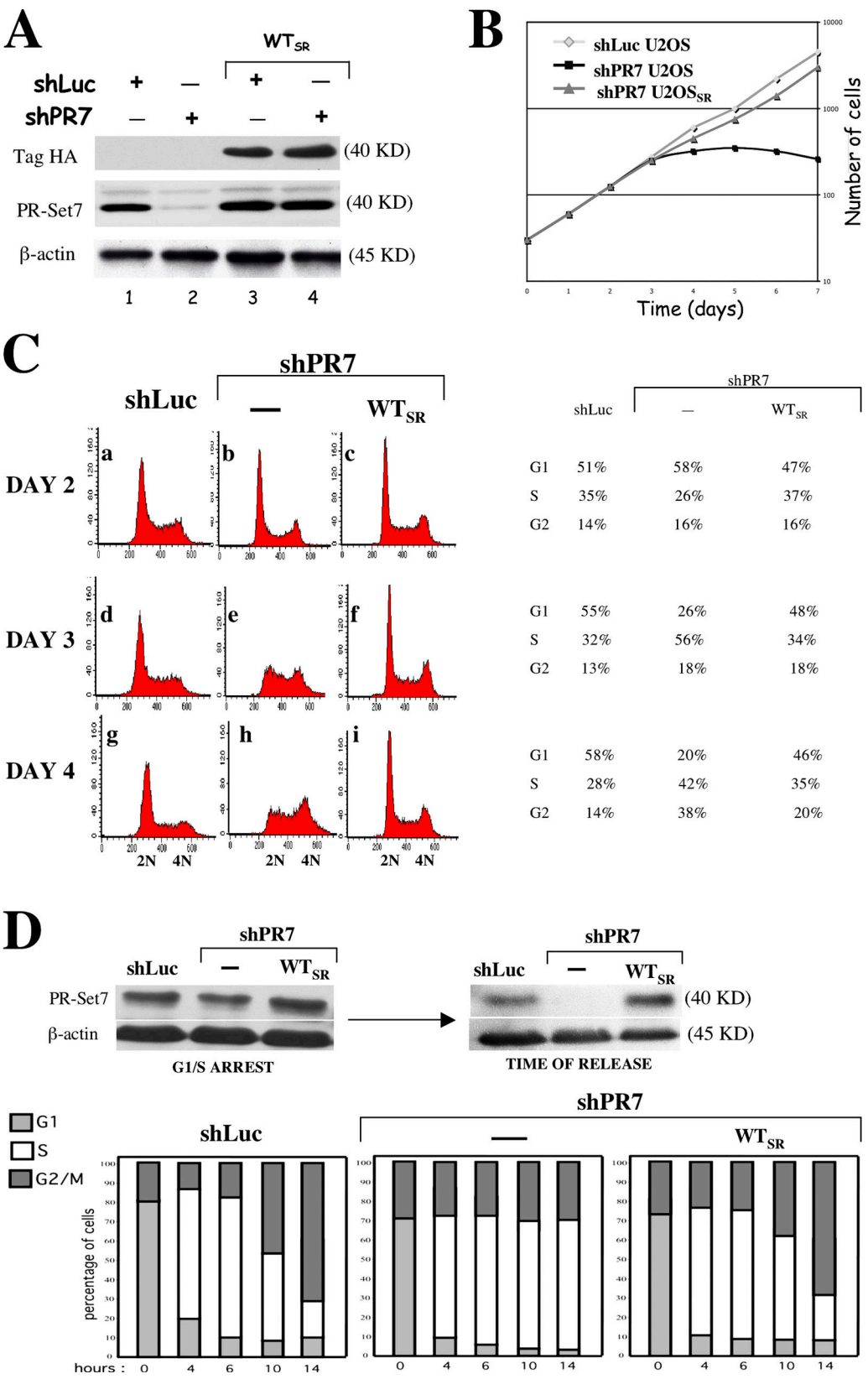

Figure 2. **PR-Set7–depleted cells display improper S-phase progression.** (A) Immunoblot analysis of U2OS cells (lanes 1 and 2) and U2OS cells synthesizing the PR-Set7$_{SR}$ recombinant protein (lanes 3 and 4) 2 d after either luciferase (lanes 1 and 3) or PR-Set7 (lanes 2 and 4) shRNA expression. shLuc for luciferase shRNA and shPR7 for PR-Set7 shRNA. The PR-Set7$_{SR}$ protein is visualized alone (HA tag antibody; top) or together with endogenous PR-Set7 proteins (middle). β-actin (bottom) is used as a loading control. Resistance to shPR7 treatment is given by five silent mutations in the mRNA sequence targeted by shPR7. (B) Proliferation rates of U2OS cells expressing either luciferase (shLuc) or PR-Set7 (shPR-Set7) shRNA and U2OS cells synthesizing PR-Set7$_{SR}$ (U2OS$_{SR}$) and expressing PR-Set7 shRNA. The proliferation rate of U2OS$_{SR}$ cells expressing luciferase shRNA is similar to shluc U2OS cells (not depicted).

cells still contained PR-Set7, as shown in Fig. 2 D (top left). 20 h later, once PR-Set7 was efficiently depleted (Fig. 2 D, top right), cells were released and pulse labeled with BrdU for 1 h at the indicated times to follow their progression through S phase. The results are shown in Fig. 2 D (bottom). 4 h after release, BrdU incorporation and DNA content of shLuc U2OS, shPR7 U2OS, and shPR7 $U2OS_{SR}$ indicated that entry into S phase was similar in the three cell populations. However shLuc U2OS and shPR7 $U2OS_{SR}$ cells underwent progression through S phase over an ~10-h time period, with ~70% of cells emerging in G2/M stage (Fig. 2 D, bottom; left and right), whereas shPR7 U2OS cells failed to complete S phase for the duration of the experiment (Fig. 2 D, bottom; middle). These results indicate that accurate completion of DNA replication is indeed directly dependent on PR-Set7 functions during S phase.

PR-Set7 silencing leads to massive DNA strand breaks during S phase and activation of a DNA damage response

Improper S-phase progression followed by a G2-phase arrest in PR-Set7–depleted cells led us to hypothesize that these cells had activated their DNA damage checkpoint. As shown in Fig. 3 A, alkaline comet assays, which monitor mainly single-strand breaks and alkali labile sites, revealed extensive DNA strand breaks in U20S cells 3 d after shPR7 expression. Close to 80% of the PR-Set7–depleted U2OS cells displayed comets with a tail moment greater than five (Fig. 3 B), whereas no significant signature of damage was observed in control cells (shLuc-treated U2OS and shPR7 $U2OS_{SR}$ cells). Strikingly, spontaneous DNA strand breakage upon PR-Set7 silencing led to a robust DNA damage response. As shown in Fig. 3 C, the molecular signature of this response was easily detectable by immunoblotting in shPR7 U2OS cellular extracts with the presence of the activated/phosphorylated forms of the DNA damage kinases ataxia telangiectasia related (ATR) and ataxia telangiectasia mutated (ATM) and their phosphorylated targets CHK1 (phosphoserine 345), H2A.X (γ-H2A.X), and p53 (phosphoserine 15). A p53-dependent response was also activated in these cells, as indicated by the sustained up-regulation of the cyclin-dependent kinase inhibitor $p21^{Waf1}$ (Fig. 3 C), a transcriptional target of p53 implicated in the maintenance of G2 arrest after DNA damage (Taylor and Stark, 2001). Importantly, this activation of the DNA damage signaling cascade was not detected in cellular extracts prepared from shLuc U2OS cells and shPR7 $U2OS_{SR}$ control cells (Fig. 3 C).

We next asked whether the DNA breaks that appeared upon PR-Set7 silencing occurred during S phase. 2 d after shLuc or shPR7 expression, U2OS and $U2OS_{SR}$ cells were synchronized at the G1/S boundary as described in Fig. 2 D and were released with fresh BrdU-containing medium 24 h later. Cells were subsequently stained with α-BrdU antiserum (to identify cells that had entered S phase) and with an antiserum against the phosphorylated form of histone H2A.X (γ-H2A.X). The results are shown in Fig. 3 D. As expected, only ~3% of shLuc U2OS cells and ~7% of shPR7 $U2OS_{SR}$ cells displayed both BrdU and γ-H2A.X staining during S-phase progression (Fig. 3 D). In contrast, whereas no γ-H2A.X staining was detected in shPR7 U2OS cells before release from the G1/S block, an intense γ-H2A.X immunostaining was observed in S phase–progressing cells, with up to 65% of BrdU-positive cells showing γ-H2A.X staining 5 h after their release (Fig. 3 D, top and bottom). Interestingly, digital sectioning images of asynchronous shPR7 U2OS cells incubated with BrdU for 10 min to detect active replication foci showed that a significant fraction of BrdU-positive foci colocalized with DNA damage foci (Fig. 3 E). A partial colocalization may lie in the fact that the appearance of DNA damage at replication foci rapidly causes the arrest of replication (Sancar et al., 2004), thereby preventing the incorporation of BrdU. Collectively, our results strongly suggest that the absence of PR-Set7 causes DNA breaks at replication sites, thereby leading to a DNA damage response characterized by activation of the ATM and ATR kinase–mediated pathways.

PR-Set7 regulates replication fork activity

The appearance of DNA breaks during S phase of PR-Set7–depleted cells could reflect some defects in replication fork activity. To adress this question, we monitored DNA replication dynamics at the level of individual DNA molecules by DNA combing experiments (Michalet et al., 1997; Pasero et al., 2002). 3 d after shLuc and shPR7 expression, we measured the velocity of replication forks by pulse labeling shRNA-treated cells consecutively with the thymidine analogues iododeoxyuridine (IdU) and chlorodeoxyuridine (CldU). Staining of combed DNA with anti-IdU and -CldU antibodies identified ongoing forks either as a stretch of IdU framed by CldU labeling or IdU label followed by a single CldU label. Representative examples of immunostaining are shown in Fig. S2 A (available at http://www.jcb.org/cgi/content/full/jcb.200706179/DC1). As shown in Fig. 4 A, quantification of the length of IdU/CldU signals indicated that the rates of elongation were dramatically reduced in PR-Set7–depleted cells (mean speed of 578 bp/min) compared with controls (750 bp/min and 892 bp/min in shPR7-treated $U2OS_{SR}$ cells and shLuc-treated U2OS cells, respectively), suggesting that replication fork velocity is impaired in the absence of PR-Set7.

We next examined the rate of initiation by measuring the density of replicated tracks in shLuc and shPR7 shRNA– treated cells, which entered into S phase synchronously. After pulse labeling cells with BrdU for 15 min, replicated tracks were detected with a BrdU antibody, and DNA fibers were counterstained with an antiguanosine antibody as shown in Fig. S2 B. Consistent with a reduction in fork velocity upon PR-Set7 depletion (Fig. 4 A),

At the indicated times, cells were harvested and counted from duplicate plates, and the results were averaged. The number of cells is represented on a logarithmic scale. (C) Cell cycle profiles of shLuc (a, d, and g) or shPR7 (b, e, and h) U2OS cells and shPR7 $U2OS_{SR}$ cells (c, f, and i). At the times indicated, cells were labeled with BrdU for 1 h before harvest and were stained with an anti-BrdU antibody and 7AAD. Only histograms of DNA fluorescence are shown. (D, top) Western blot analysis for PR-Set7 and β-actin levels in U2OS and $U2OS_{SR}$ cells arrested at G1/S stage by thymidine block 2 d after shRNA expression and released into S phase 20 h later. (bottom) Cell cycle distribution of shLuc (left) or shPR7 U2OS cells (middle), and shPR7 $U2OS_{SR}$ cell (right) release into S phase from a thymidine block (0 h) and pulse labeled for 1 h with BrdU at the times indicated below each panel. The percentage of cells in each stage of the cell cycle was monitored by measuring BrdU incorporation and DNA content with a flow cytometer in three independent experiments.

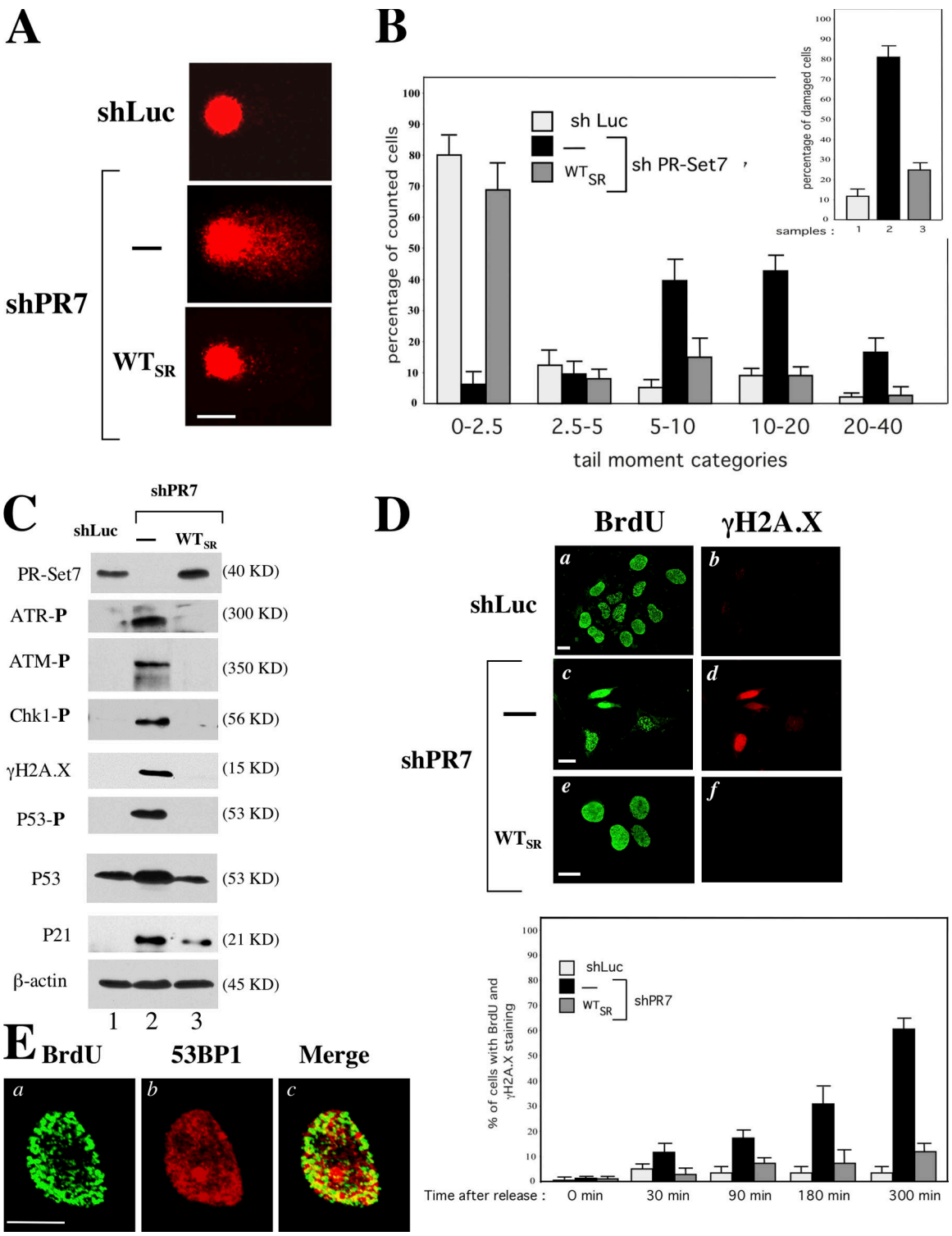

Figure 3. **PR-Set7 silencing causes massive DNA breaks during S phase, which leads to activation of the DNA damage checkpoint.** (A) Representative comets of shLuc and shPR7 U2OS cells and shPR7 $U2OS_{SR}$ cells. Alkaline comet analysis was performed 3 d after shRNA expression. At least 200 randomly chosen comets were captured. (B) Distribution of cells with different comet tail moments and quantification of the number of cells with comet tail moments greater than five (inset) are illustrated for each cell line. The tail moment and distribution were scored from 200 cells/slide by using Comet Imager 1.2.10 software. (C) Immunoblot analysis of the total levels of p53 and P21 and the levels of phosphorylation of ATM, ATR, CHK1, H2A.X, and p53 in U2OS (lanes 1 and 2) and $U2OS_{SR}$ (lane 3) cells 3 d after either shLuc (lane 1) or shPR7 (lanes 2 and 3) expression. (D) Immunofluorescence of BrdU (a, c, and e) and γ-H2A.X (b, d, and f) in shLuc and shPR7 U2OS cells and shPR7 $U2OS_{SR}$ cells 3 h after release from a thymidine block. (bottom) Quantification of double BrdU and γ-H2A.X–positive cells in shRNA-expressing U2OS and $U2OS_{SR}$ cell lines. Cells were harvested and analyzed by immunofluorescence at the times indicated. The percentages of double BrdU and γ-H2A.X–positive cells were obtained by counting 300 cells from three independent experiments. Error bars represent SD. (E) Images of asynchronous shPR7 U2OS nuclei acquired with Apotome microscopy 3 d after shRNA expression. After BrdU incorporation for 10 min, cells were stained with anti-BrdU antibody to detect active replication foci (a) and anti-53BP1 antibody to detect DNA damage foci (b). The merged picture (c) showed a partial but significant overlay. Bars, 5 μm.

the length of the replicated tracks was shorter in shPR7 U2OS cells than in shLuc U2OS and shPR7 $U2OS_{SR}$ cells (Fig. 4 B). Furthermore, the number of replicated tracks was severely reduced in shPR7 U2OS cells (Fig. 4 C), and, accordingly, the mean distance between these tracks was longer in these cells (Fig. 4 D). Thus, in addition to a reduction in fork velocity, PR-Set7–depleted cells display a decrease in the density of active replication forks.

These results were surprising because a decrease in fork velocity is often compensated by an increase in replication fork density (Anglana et al., 2003). We assumed that this might reflect the inhibition of late replication origins by the ATR and ATM kinase pathways in response to DNA damage (Sancar et al., 2004). To test this hypothesis, replication fork activity (Fig. 4, B–D) and cell cycle progression (Fig. 4 E) were analyzed in shPR7 U2OS cells that were treated for 5 h with 10 mM caffeine (an inhibitor of ATM and ATR kinases). Although the length of replicated tracks remained severely reduced in these caffeine-treated shPR7 U2OS cells (Fig. 4 B, bottom), the density of their active replication forks was largely increased (Fig. 4, C [bar 4] and D), and they were then able to bypass S-phase arrest upon PR-Set7 depletion (Fig. 4 E). Thus, these results support a scenario in which the absence of PR-Set7 at replication foci impairs the progression of the replication machinery, leading to DNA breaks and activation of a DNA damage response that delays S-phase progression by regulating the origin-firing timing.

The p53 response induced by DNA damage in PR-Set7–depleted cells is required to prevent aberrant mitotic chromosome behavior

Inactivation of the *Drosophila* PR-Set7 orthologue also causes an activation of a DNA damage response in neuroblasts of the third instar larval brains (Sakaguchi and Steward, 2007). However, in contrast to our results, this activation is associated with extensive mitotic defects, including improper mitotic chromosome structure and progression (Karachentsev et al., 2005; Sakaguchi and Steward, 2007). In our case, we did not observe significant alterations of these mitotic events in shPR7 U2OS cells (unpublished data). This might reflect the fact that the *Drosophila* p53 orthologue does not possess the growth arrest functions like its mammalian counterpart (De Nooij and Hariharan, 1995; Sogame et al., 2003).

To address this point, we investigated whether human p53 was required to prevent the onset of mitosis in PR-Set7–depleted cells that were able to exit S phase with DNA damage. Thus, shRNA-mediated depletion of PR-Set7 was performed in HNFs or in the same cells expressing the human papillomavirus oncoprotein E6 (HNF_{E6}), which targets p53 for degradation (Scheffner et al., 1993). Although E6 has targets other than p53, HNF_{E6} cells are commonly used as a human cellular model deficient for p53 functions (Baus et al., 2003; Mallette et al., 2007). As shown in Fig. 5 A, cell cycle profile analyses showed that both shPR7 HNF and shPR7 HNF_{E6} cells gradually accumulated in S phase and then in the G2/M stage 3 d after shRNA expression. Consistent with our data in U20S cells, none of the shPR7 HNF cells with DNA damage had entered into mitosis, as indicated by the fact that we did not detect fluorescent co-immunostaining of these cells probed with the DNA damage marker γ-H2A.X and the mitotic marker phosphohistone H3-S10 (unpublished data). In contrast, this costaining was readily observed in ∼90% of shPR7 HNF_{E6} mitotic cells, as shown in Fig. 5 B. Strikingly, these cells displayed abnormal mitotic chromosome morphology (Fig. 5 B).

To document this observation, we prepared chromosome spreads after a 30-min colchicine treatment and hypotonic shock. As illustrated in Fig. 5 C, shLuc mitotic cells showed clearly defined sister chromatids (panel a). In contrast, most of chromosome spreads of shPR7 mitotic HNF_{E6} showed either defective chromosome condensation (∼80%) as shown in Fig. 5 (C, b and c) or condensed chromosomes (∼20%) but with a significant number of aberrations, including chromosome breaks (Fig. 5 C; d, d-1, d-2, and d-3) and sister chromatid fusion (Fig. 5 C; d and d-4). Conspicuously, such mitotic defects are reminiscent of those observed in *Drosophila* PR-Set7–depleted neuroblasts (Sakaguchi and Steward, 2007). These data illustrate the importance of the DNA damage–induced p53 response to prevent abnormal chromosome behavior upon PR-Set7 depletion in human cells.

PR-Set7 depletion in U2OS cells is associated with reduced levels of H4-K20 mono- and trimethylation

To gain insights into the mechanisms by which PR-Set7 regulates DNA replication and genome stability, we examined the levels of H4-K20 methylation in PR-Set7–depleted cells displaying improper S-phase progression. 3 d after shRNA expression, total histones of U2OS and $U2OS_{SR}$ cells were acid extracted and subjected to immunoblot analysis with the different antimethylated H4-K20 antibodies. The results are shown in Fig. 6 A. The levels of the three methyl marks were similar between shLuc U2OS and shPR7 $U2OS_{SR}$ cells (Fig. 6 A). In contrast, the levels of H4-K20me1 as well as of H4-K20me3 were strongly reduced in shPR7 U2OS cells, suggesting that PR-Set7 plays a key role in the maintenance of both H4-K20 mono- and trimethyl marks during S phase. For H4-K20me2, we observed only a slight reduction in shPR7 U2OS cells (Fig. 6 A), suggesting that changes in H4-K20me2 levels are not associated with the DNA replication defects described here. Consistent with the preservation of H4-K20me2 in PR-Set7–depleted U2OS cells, p53-binding protein 1 (53BP1), which associates primarily with H4-K20me2 in response to DNA damage (Botuyan et al., 2006), was still colocalized with spontaneous as well as irradiation-induced DNA damage foci (Fig. S3, available at http://www.jcb.org/cgi/content/full/jcb.200706179/DC1).

Repeated siRNA-mediated depletion of PR-Set7 in HeLa cells was reported by others to result in the disappearance of H4-K20me2 (Botuyan et al., 2006). Consistent with this study, we also observed a clear reduction in H4-K20me2 levels in shPR7-treated HeLa cells, but at least 2 d after the decrease of H4-K20me1 and H4-K20me3 (Fig. S4, available at http://www.jcb.org/cgi/content/full/jcb.200706179/DC1). However, in strike contrast with our results in U2OS cells and normal fibroblasts, HeLa cells continue to proliferate after PR-Set7 depletion (Fig. S4;

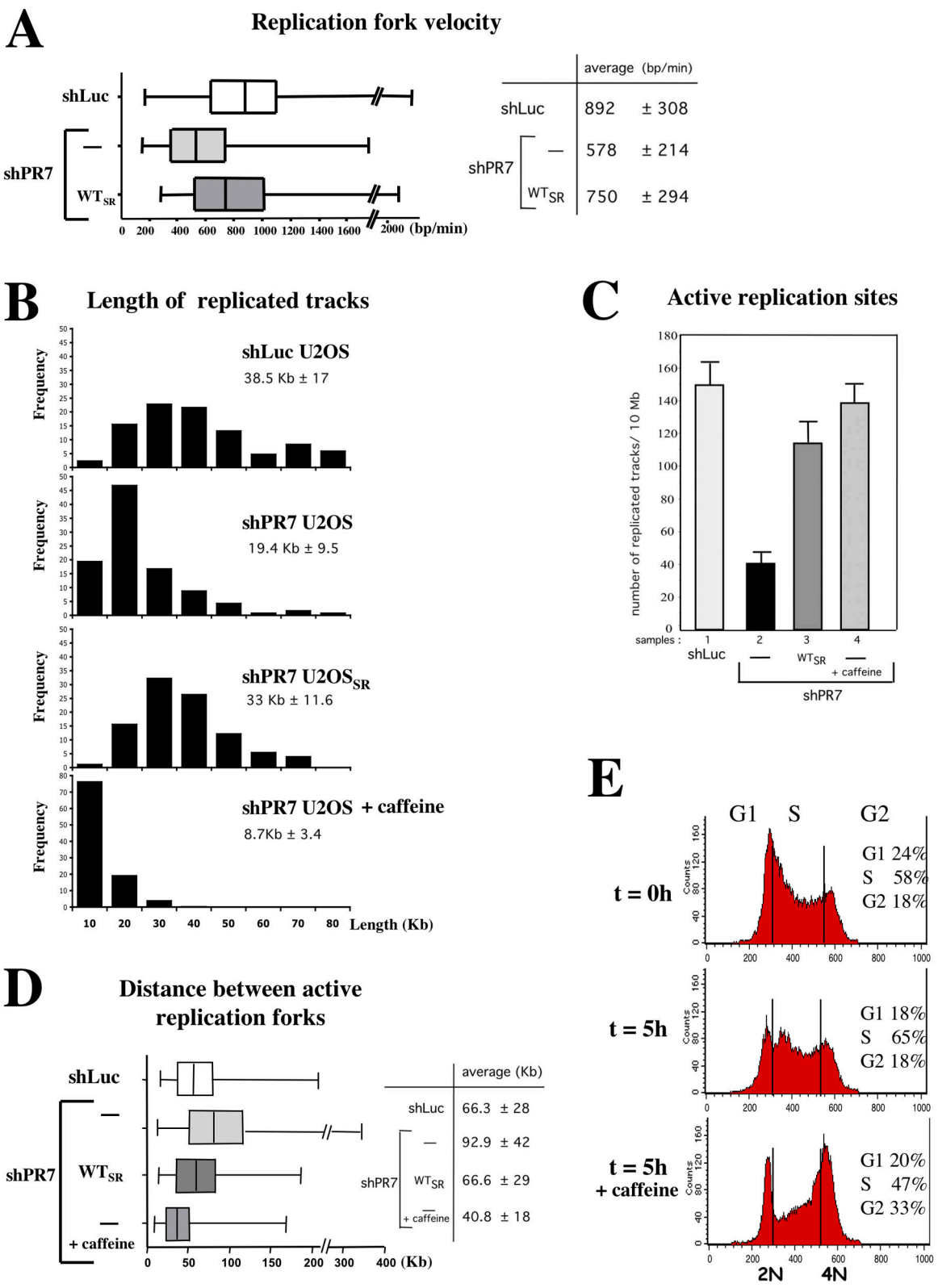

Figure 4. **PR-Set7 regulates replication fork activity.** (A) Distribution of fork velocity from 200 ongoing replication forks in shLuc or shPR7 U2OS cells and in shPR7 U2OS$_{SR}$ cells (left). Squares represent the quartiles (25% of the fork rate values smaller and higher than the median value), and the deviations show the smallest and greatest fork rate values. Mean fork rates with SDs are indicated for each sample (right). $P < 0.0002$ as determined by the nonparametric test of Mann-Whitney. (B) Distribution of replicated track lengths after 30 min of BrdU incorporation in shLuc U2OS (top), shPR7 U2OS and U2OS$_{SR}$ cells (middle), and shPR7 U2OS treated with caffeine for 5 h (bottom). Mean lengths with SDs are indicated for each panel. Results were averaged from five independent experiments. (C) Quantification of active replication sites for 10 Mb DNA in BrdU-positive shLuc (bar 1) or shPR7 (bar 2) U2OS cells, BrdU-positive shPR7 U2OS$_{SR}$ cells (bar 3), and BrdU-positive shPR7 U2OS cells treated with caffeine for 5 h (bar 4). The number of active replication sites was obtained by counting the number of individual BrdU tracks for 10 Mb DNA 3 d after shRNA expression in five independent DNA combing experiments.

Julien and Herr, 2004). This continued cell cycle progression upon PR-Set7 depletion likely reflects the fact that the genetic and growth properties of HeLa cells are highly altered by oncogenic transformation. Therefore, we assume that the reduction of H4-K20me2 levels is a late and indirect event that can be observed only in cells that continue to proliferate upon PR-Set7 depletion. Thus, these results suggest that the DNA replication defects and DNA breaks observed in PR-Set7–depleted U2OS cells are primarily associated with a global loss of the K20me1 and K20me3 methylated forms of histone H4.

PR-Set7–mediated lysine methylation is essential for S-phase progression and genomic stability

To further demonstrate that loss of the histone methyltransferase activity of PR-Set7 is indeed the key event that causes defective DNA replication and genomic instability during S phase, we examined the ability of shRNA-resistant PR-Set7 (PR-Set7$_{SR}$) mutants to rescue the PR-Set7 loss of function phenotype. Fig. 6 B shows the structure of the different PR-Set7$_{SR}$ mutants tested. Among them, only PR-Set7$_{SR/\Delta 141–322}$ deleted for the SET domain and PR-Set7$_{SR/R265G,}$ which contains an arginine to glycine substitution at position 265 within the entire SET domain, lack PR-Set7 methyltransferase activity (Nishioka et al., 2002).

The PR-Set7$_{SR}$ mutants were stably expressed in U2OS cells and infected with either shLuc or shPR7 retrovirus. 4 d after shRNA expression, we monitored (1) defective S-phase progression by measuring the levels of BrdU incorporation and DNA content by flow cytometry and (2) DNA damage by immunofluoresence with γ-H2A.X staining. The results are shown in Fig. 6 (C and D, respectively). Importantly, the different PR-Set7 mutants themselves did not induce defective cell cycle progression and DNA breaks compared with untransfected cells (unpublished data). As expected, PR-Set7 inhibition led to an accumulation of cells in S and G2/M stages associated with DNA breaks (Fig. 6, C and D). Analysis of the different PR-Set7$_{SR}$ mutants reveals that PR-Set7 methyltransferase activity is essential to preserve genome stability and proper DNA replication. Wild-type PR-Set7$_{SR}$ as well as PR-Set7$_{SR/\Delta 1–30}$, PR-Set7$_{SR/\Delta 37–50}$, and PR-Set7$_{SR/\Delta 51–140}$ (Fig. 6 D, bars 2–5) were generally successful in rescuing both normal S-phase progression (Fig. 6 D) and genome stability (Fig. 6 D), whereas PR-Set7$_{SR/\Delta 141–322}$ and PR-Set7$_{SR/R265G}$ were not (Fig. 6 D, bars 6 and 7). Collectively, these results indicate that PR-Set7–mediated lysine methylation, likely H4-K20me, is essential for the accurate completion of DNA replication and for preservation of genome integrity through S phase.

Discussion

In this study, we provide evidence that the histone H4-K20 methyltransferase PR-Set7 plays a key role during S phase in normal as well as in transformed human cells. Consistent with a role in DNA replication and in the maintenance of chromosome integrity during S phase, we have shown that PR-Set7 localizes with sites of DNA synthesis and regulates the bulk of histone H4-K20 methylation. Inhibition of PR-Set7 by shRNA causes (1) alterations in the number and velocity of active replication forks and (2) massive induction of DNA strand breakage followed by a robust DNA damage response. This DNA damage response includes the activation of ATM and ATR kinase–mediated pathways, which leads to a p53-mediated growth arrest in G2 to avoid aberrant chromosome behavior after improper DNA replication.

To characterize the PR-Set7 loss of function phenotype in mammalian cells, we used shRNA viral vectors to silence PR-Set7 expression. The main limitation of this approach is the off-target effects of the shRNA sequences (for review see Cullen, 2006). Therefore, we created shRNA-resistant wild-type PR-Set7 molecules in U2OS cells and sucessfully rescued all aspects of the PR-Set7 loss of function phenotype. Finally, the use of mutant shRNA-resistant PR-Set7 molecules revealed that the PR-Set7 methyltransferase activity was essential for genome replication and stability through S phase.

Regulation of H4-K20 methylation levels by PR-Set7

In mammalian cells, mono- and trimethylation of H4-K20 appear relatively stable during the cell cycle, whereas dimethylation follows a cyclic pattern with maximum levels in S phase, suggesting that H4-K20me1 and H4-K20me3 are regulated differently than the dimethyl mark (Fang et al., 2002; Karachentsev et al., 2007). Accordingly, our results in U2OS cells indicate that PR-Set7 functions during S phase are important for the maintenance of H4-K20me1 and H4-K20me3 but not for H4-K20me2 (Fig. 6). A role for PR-Set7 in the regulation of H4-K20me3 was unexpected because this enzyme is clearly defined as a methyltransferase that specifically monomethylates histone H4-K20 (Couture et al., 2005; Xiao et al., 2005), whereas H4-K20me3 was triggered by the Suv4-20h1 and Suv420h2 enzymes (Schotta et al., 2004). Importantly, the levels of Suv4-20h1 and Suv420h2 are not altered in PR-Set7– depleted cells (unpublished data), indicating that the decrease in H4-K20me3 is likely caused by loss of the monomethyl mark. This interdependence between the lysine mono- and trimethylation state, as suggested here for histone H4-K20, has been previously described for another mark of silent chromatin domains, histone H3-K9me (Peters et al., 2003; Schotta et al., 2004). In this case, the H3-K9 trimethylating enzymes appear to use an H3-K9 monomethyl residue as their in vivo substrate (Peters et al., 2003). Accordingly, knockout of the H3-K9 trimethylating enzymes in mouse embryonic stem cells resulted in a significant decrease in H3-K9me3 and, conversely, an increase in H3-K9me1 (Peters et al., 2003, Schotta et al., 2004). Although the

Error bars represent SD. (D) Distances between replicated tracks labeled with BrdU in shLuc and shPR7 U2OS cells, shPR7 U2OS$_{SR}$ cells, and shPR7 U2OS cells treated with caffeine for 5 h. The mean distances with SDs are indicated (right). (B and D) $P < 0.0001$ as determined by the nonparametric test of Mann-Whitney. (E) Cell cycle profiles of shPR7 U2OS cells untreated or treated with caffeine 3 d after shRNA expression. At the starting time point (top), cells were untreated (middle) or treated (bottom) with caffeine, and, 5 h later, they were labeled with BrdU before harvest and stained with an anti-BrdU antibody and 7AAD. Only histograms of DNA fluorescence are shown.

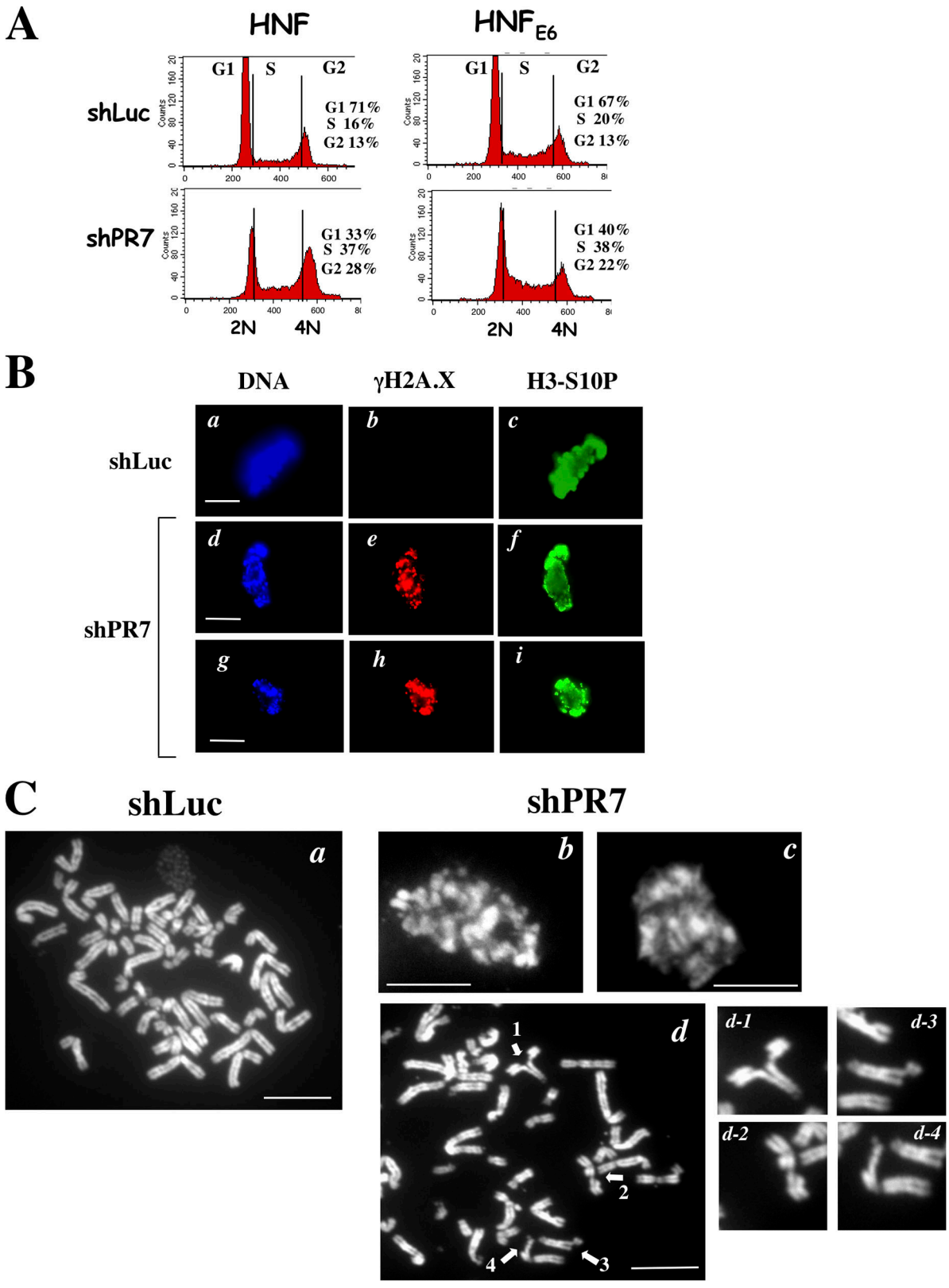

Figure 5. **Growth-arrest functions of p53 avoid aberrant mitotic chromosome behavior after improper DNA replication in PR-Set7–depleted cells.** (A) Cell cycle profiles of HNF and HNFE6 4 d after shLuc or shPR7 expression. Histograms of DNA content are shown. (B) Immunofluorescence analysis of mitotic HNFE6 4 d after shLuc (a–c) or shPR7 (d–i) expression. DAPI staining (a, d, and g), H2A.X staining (b, e, and h), and phosphorylated histone H310 staining (c, g, and j) are shown. Note the abnormal DAPI staining in shPR7 HNFE6. (C) Chromosome spreads of shLuc (a) and shPR7 (b–d) HNFE6. (b and c) Examples of mitotic shPR7 HNFE6 showing improper chromosome condensation. (d1–4) Magnification of the selected areas from panel d showing chromosomal aberrations in shPR7 HNFE6. Bars: (B) 5 μm; (C) 2.5 μm.

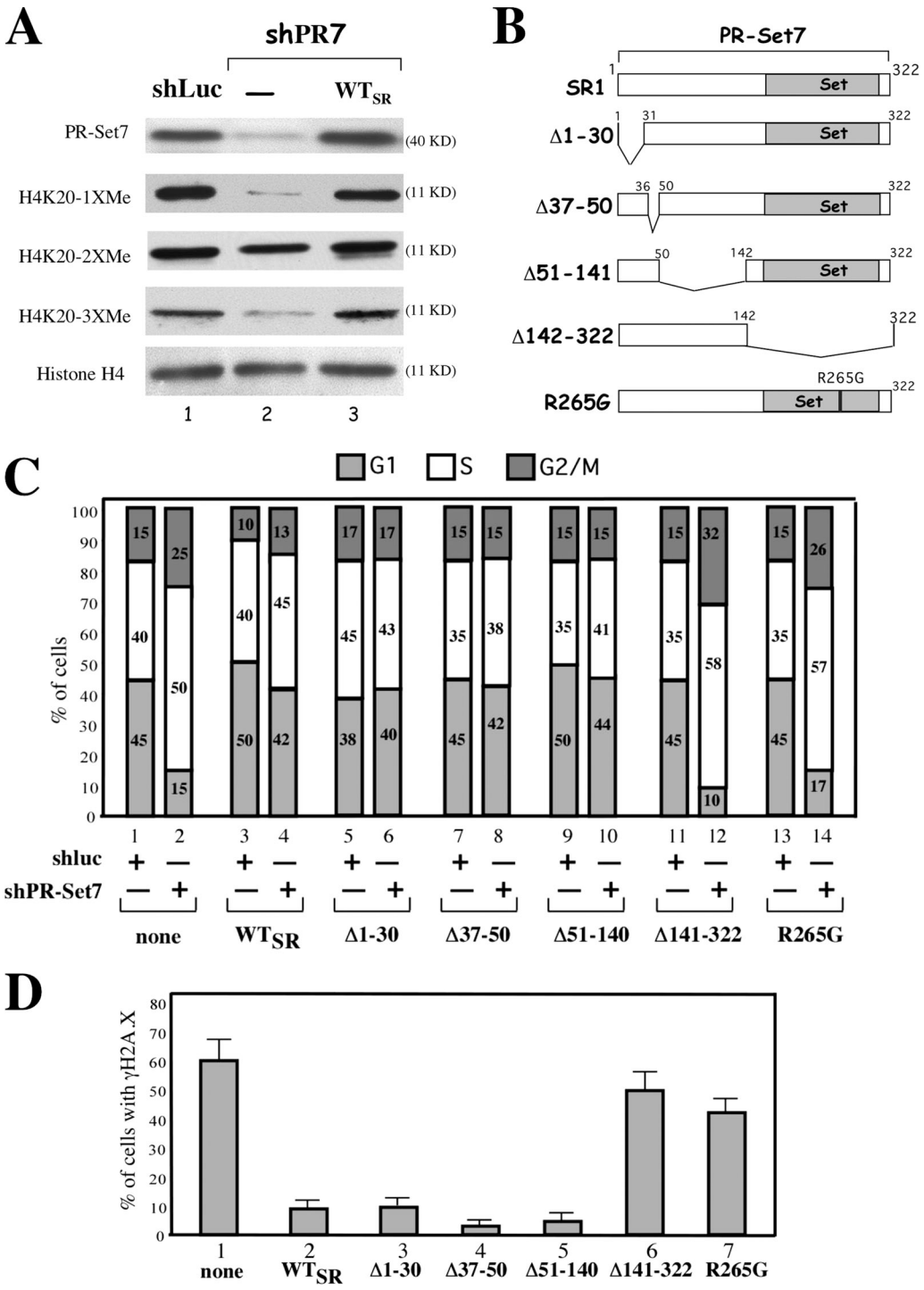

Figure 6. **PR-Set7 regulates H4-K20 mono- and trimethylation, an essential function for proper S-phase progression and genomic stability.** (A) Immunoblot analysis of the levels of PR-Set7, histone H4, H4-K20me1, H4-K20me2, and H4-K20me3 in U2OS and $U2OS_{SR}$ cells 3 d after shLuc or shPR7 expression. (B) Schematic structures of the shRNA-resistant wild-type (SR1), truncated (Δ1–30, Δ37–50, Δ51–140, and Δ141–322), and mutated (R265G) PR-Set7 recombinant proteins. (C) Cell cycle distribution of parental cells (bars 1 and 2) or cells synthesizing the indicated shRNA-resistant PR-Set7 recombinant proteins (bars 3–14) 3.5 d after shLuc (odd-numbered bars) or shPR7 (even-numbered bars) expression. The percentage of cells in each stage of the cell cycle is shown and was obtained by measuring BrdU incorporation (1-h pulse labeling before harvest) and DNA content with flow cytometry in three independent experiments. (D) Quantification of γ-H2A.X–positive cells in parental U2OS cells and cells synthesizing the indicated shRNA-resistant PR-Set7 recombinant proteins 3.5 d after shPR7 expression. The percentage of γ-H2A.X cells was obtained by counting 100 cells in three independent experiments. No γ-H2A.X signal was detected in the different PR-Set7 recombinant–expressing cell lines untreated or treated with luciferase shRNA (not depicted). Error bars represent SD.

PR-Set7 loss of function phenotype described here provides the first evidence that this scenario might also apply to H4-K20me, it will be important to study the phenotype of the loss of function of *Suv4-20h* genes to fully address this question, a compound model that is now available (Benetti et al., 2007).

PR-Set7 functions during DNA replication

An important finding of our studies is that PR-Set7–depleted cells can initiate DNA replication, at least during early S phase, but then they fail to proceed properly with the elongation step of DNA replication. How might PR-Set7 ensure proper replication fork progression? In *Drosophila*, the PR-Set7 orthologue suppresses position effect variegation (Nishioka et al., 2002; Karachentsev et al., 2005), raising the possibility that it functions as a transcriptional repressor. Although we cannot exclude that mammalian PR-Set7 may indirectly promote replication fork progression by regulating gene expression, localization of the enzyme at sites of DNA synthesis (Fig. 1) and our results with synchronized cells (Fig. 2 D) support a model in which PR-Set7 would directly participate in the replication machinery. Intriguingly, our results show that localization of PR-Set7 at replication foci is strongly enhanced upon proteasome inhibition (Fig. 1), suggesting a rapid exchange of the pool of PR-Set7 proteins associated with these foci during S phase. The biological significance of this proteasome-mediated turnover of PR-Set7 is still unclear; however, our current hypothesis is that this might represent a novel and important regulatory step in the control of DNA replication. Among many other possible scenarios, this might be linked with rapid and local changes of chromatin structure that are necessary for the activation and displacement of replication forks along the DNA template (Nishitani et al., 2006; Senga et al., 2006).

Recruitment of a histone methyltransferase to sites of DNA synthesis is not unprecedented, as it has been observed for the histone H3-K9 methyltransferases G9a (Esteve et al., 2006) and SETDB1 (Sarraf and Stancheva, 2004). This is thought to contribute to the restoration of H3-K9 methylation patterns on newly assembled chromatin behind the replication fork. A similar function of PR-Set7 in the maintenance of H4-K20 methylation patterns during S phase would be consistent with our data and would notably explain why PR-Set7 inhibition causes an acute DNA replication stress. Indeed, structural analysis of nucleosomal particles revealed that the position of K20 within the N-terminal tail of histone H4 makes an interparticle contact between the histone H2A-H2B dimer and DNA (Davey et al., 2002), an observation that suggests that methylation of this lysine can directly affect the nucleosome structure. Furthermore, it has been recently shown that binding of the protein L3MBTL1 to nucleosomes is directly regulated by the specific methylation state of H4-K20 (Trojer et al., 2007), which is thought to contribute to chromatin compaction. Therefore, alterations in H4-K20 methylation could result in a rapid regulatory dead end for the packaging of nascent DNA into chromatin, thereby leading to the generation of DNA breaks, as we have observed in PR-Set7–depleted cells.

An alternative but not mutually exclusive possibility is that PR-Set7 may also modify other components of chromatin, including the replication machinery itself, that are essential for proper replication fork progression and stability. For example, the acetyltransferase HBO1, which is required for S-phase initiation and fixing replication origins (Doyon et al., 2006), can acetylate histone H4 as well as replication proteins (Iizuka et al., 2006). Recently, PR-Set7 has been reported to monomethylate the tumor suppressor p53 at lysine 382, which represses p53 transcriptional activation on a subset of target genes (Shi et al., 2007). Importantly, inhibition of p53-K382me without affecting H4-K20me did not cause any growth defects in U2OS cells (Shi et al., 2007), suggesting that abnormal PR-Set7–mediated methylation of p53 is not the prime cause of the replication defects described here. Other nonhistone targets of PR-Set7 have not been identified yet, and further work will be necessary to identify such targets. If they exist, it will be of great interest to determine whether their methylation plays a role in genome replication and stability.

Does PR-Set7 play a role in tumorigenesis?

The S phase of the cell cycle is a period of high vulnerability for the genome. Either intrinsic or external events can lead to the stalling of replication forks, which, if not managed properly, can have devastating consequences for the integrity of the genome. Indeed, there is now clear evidence that DNA damage during S phase can lead to genomic instability, thereby creating clones of cells that proliferate uncontrollably (Bartkova et al., 2005; Gorgoulis et al., 2005). Our findings that PR-Set7 catalytic activity ensures proper DNA replication and stability during S phase suggest that PR-Set7–mediated lysine methylation is a safeguarding posttranslational modification for the genome. This is particularly evident in cells defective for the tumor suppressor p53 and depleted from PR-Set7, in which improper DNA replication and generation of DNA damage lead to aberrant mitotic chromosome behavior (Fig. 5), a hallmark of cancer cells (for review see Duesberg and Li, 2003). Given the importance of deregulated DNA replication in tumorigenesis (Bartkova et al., 2006; Di Micco et al., 2006) and that loss of H4-K20me3 patterns are observed in almost all human cancers (Fraga et al., 2005), it will be interesting to explore whether PR-Set7 is a putative target for cellular transformation and contributes to tumor development.

Materials and methods

Cell lines and synchronization

U2OS cells and HNFs, either wild type or expressing the viral oncoprotein E6 (gift from J. Piette and V. Gire, Centre de Recherche en Biochimie Macromoléculaire, Montpellier, France), were grown in DME with 10% FBS (Invitrogen) supplemented with penicillin and streptomycin. Synchronization of U2OS cells at the G1/S boundary was performed by a double thymidine block. Cells were first blocked with 2.5 mM thymidine for 15 h, released for 8 h, and then blocked again with 2.5 mM thymidine for 15 h. To control the efficiency of synchronization, flow cytometry analysis was performed.

shRNA preparation and transfection

A human PR-Set7 shRNA directed against the PR-Set7 mRNA sequence GATGCAACTAGAGAGACA (nucleotides 854–871) was checked against the human genome sequence to ensure that only the PR-Set7 mRNA would be targeted. A firefly luciferase nonspecific control shRNA was used. The shRNA sequences were introduced into the puromycin retroviral vector RNAi Ready pSiren (BD Biosciences) according to the manufacturer's instructions. Cells were infected with the corresponding retroviral particles as described previously (Le Cam et al., 2006) and were selected 24 h later in 10 μg/ml puromycin.

Mutagenesis and generation of PR-Set7$_{SR}$ cell lines

A hygromycin retroviral vector pMSCV was modified to encode the HA epitope tag downstream of the ATG, creating pMSCV-HA vector. The HA

epitope tag sequence is followed by an SpeI–BamH1 polylinker. Spe1–BamH1 cDNA fragments encoding the different PR-Set7 truncations were cloned into pMSCV-HA vector. The PR-Set7$_{SR}$ constructs were prepared by introducing five silent mutations into PR-Set7 cDNA as described previously (Julien and Herr, 2003). For stable PR-Set7$_{SR}$ expression, U2OS cells were infected as described previously (Le Cam et al., 2006) and selected with 60 μg/ml hygromycin B.

Flow cytometry

Cells were incubated with 300 μM BrdU (Sigma-Aldrich) for 1 h, fixed with a 70% ethanol solution, and permeabilized with 0.2% Triton X-100 for 10 min. Then, cells were treated with 0.2 N HCl before staining with mouse antibody to BrdU (1:30 diluted in PBS with 0.2% Tween 20 and 1% BSA; Becton Dickinson) for 1 h at room temperature followed by 1-h incubation with an FITC-conjugated antibody (1:300; BD Biosciences). DNA was then counterstained by overnight incubation with 7-amino-actinomycin D (7AAD; 1:50; Sigma-Aldrich) in the presence of RNase. Cell cycle profiles were analyzed by a flow cytometer (FACScan; Becton Dickinson) using CellQuest software (Becton Dickinson).

Western blot analysis

For immunoblot analysis, cells washed with PBS were lysed in laemmli buffer (for histones, acid extraction was performed according to the Abcam protocol). After measuring protein quantity by Bradford, equal amounts of protein were resolved by SDS-PAGE, transferred to a nitrocellulose membrane (Whatman), and probed with one of the following antibodies: mouse antiphospho-ATM-Ser1981 (1:1,000; Cell Signaling Technology), rabbit antiphospho-ATR-Ser428 (1:1,000; Cell Signaling Technology), rabbit antiphospho-Chk1-Ser345 (1:1,000; Cell Signaling Technology), mouse anti-Chk1 (1:1,000; gift from V. Gire), rabbit anti-p21 (1:500; gift from V. Dulik, Institut de Génétique Moléculaire, Montpellier, France), rabbit antiphospho-p53-Ser15 (1:500; gift from V. Gire), mouse anti-p53 (1:1,000; gift from V. Gire), rabbit anti–PR-Set7 (1:1,000; Millipore), mouse anti–β-actin (1:20,000; Sigma-Aldrich), mouse antiphospho-H2A.X-Ser139 (1:1,000; Millipore), rabbit antiphospho-histone H3-Ser10 (1:1,000; Millipore), rabbit anti–H4-K20-1xMe, -2xMe, or -3xMe (1:1,000; Millipore), rabbit anti–histone H4 (1:1,000; Millipore), and mouse anti-HA tag (12CA5; Cold Spring Harbor Laboratory). Membranes were then incubated with the appropriate HRP-conjugated secondary antibodies. The immunoreactive bands were detected by chemiluminescence (Thermo Fisher Scientific).

Immunofluorescence

For immunofluorescence, shRNA-infected cells grown on glass coverslips were fixed in 3% PFA for 15 min, permeabilized with 0.2% Triton X-100 in PBS for 15 min, and blocked for 1 h with 1% BSA (Roche) at room temperature. To visualize PR-Set7, cells on coverslips were pretreated with 15 μM MG132 for 1 h and incubated for 10 min at 4°C with a solution of PBS and 0.5% Triton X-100 before PFA fixation. Incubation with primary antibodies against PR-Set7 (1:600; Millipore), HA tag (12CA5; 1:500), phospho-H2A.X-Ser139 (1:500; Millipore), phosphohistone H3-Ser10 (1:600; Millipore), proliferating cell nuclear antigen (1:500; gift from J. Piette), DNA polymerase ε (1:800; gift from D. Fischer, Institut de Génétique Moléculaire, Montpellier, France), and 53BP1 (1:500; Millipore) was conducted at room temperature for 1 h. After washing, cells were incubated with AlexaFluor568- or 488-conjugated goat anti–mouse or goat anti–rabbit secondary antibodies (Invitrogen) for 1 h. Cells were finally stained with DAPI, and coverslips were mounted using Prolong Antifade (Invitrogen). Samples were examined at room temperature with a microscope (Imager. Z1; Carl Zeiss, Inc.) equipped with a 63× NA 1.4 or 40× NA 1.25 oil immersion objective and an Apotome device (Carl Zeiss, Inc.). Pictures were captured using a camera (CoolSNAP HQ^2; Photometrics) interfaced with MetaMorph software 7.1 (MDS Analytical Technologies), and levels were adjusted with Photoshop 7 (Adobe). Digital sectioning images (Apotome) were captured using Axiovision 4.6 software (Carl Zeiss, Inc.).

Chromosome spreading

3 d after shPR7 or shLuc expression, HNF$_{E6}$ cells were incubated for 30 min with 10 μg/ml colchicine. After washing in PBS, cells were resuspended in a hypotonic solution of 75 μM KCl for 15 min at 37°C. They were then fixed twice with a methanol/acetic acid buffer for 10 min at 4°C and spotted on frozen microscope glass slides. After drying, slides were stained with a solution of PBS and 0.1% Tween 20 containing Hoescht (1:10,000) mounted using Prolong Antifade, and images were captured at room temperature using an Imager.Z1 microscope with a 100× NA 1.4 oil immersion objective (Carl Zeiss, Inc.) equipped with a CoolSNAP HQ^2 camera interfaced with MetaMorph software 7.1. Levels were adjusted with Photoshop 7.0.

DNA combing

U2OS cells were pulse labeled for 15 min with 50 μM BrdU and were harvested. For IdU-CldU labeling experiments, cells were successively labeled for 1 h with 25 μM IdU and 200 μM CldU for 1 h. Nuclei (from ~2.5 × 10^4 cells) were embedded in agarose plugs, stained with YOYO-1 (Invitrogen), and resuspended in 50 mM MES, pH 5.6, after digestion of the plugs with agarase (Roche). Then, DNA combing was performed as described previously (Michalet et al., 1997). In brief, combed DNA fibers were denatured for 25 min with 0.2 N NaOH, and BrdU and CldU were detected with a rat anti-BrdU antibody (clone BU-75; Sera Laboratory) and a secondary antibody coupled to AlexaFluor488 (Invitrogen). IdU was detected with a mouse monoclonal anti-IdU antibody (clone B44; Becton Dickinson) and a secondary antibody coupled with AlexaFluor546 (Invitrogen). DNA molecules were counterstained as previously described (Pasero et al., 2002) with an antiguanosine antibody (Argene) and an anti–mouse IgG coupled to AlexaFluor546 (Invitrogen). DNA fibers were examined, and images were captured at room temperature using a microscope (DMRX; Leica) with a 40× NA 1.25 oil immersion objective (Leica) and equipped with a CoolSNAP FX camera interfaced with MetaMorph software 7.1. Levels were adjusted with Photoshop 7.0. Replicated track sizes were measured with MetaMorph using adenovirus DNA molecules as a size standard (one pixel = 680 bp). Fork speed was calculated by dividing track sizes by labeling time, and the nonparametric test of Mann-Whitney was used.

Comet assay

DNA break repair was assayed by alkaline single-cell agarose gel electrophoresis essentially as described previously (Murr et al., 2006). In brief, cells were infected with shRNA luc (control) or shRNA PR-Set7, harvested (~10^5 per pellet) 5 d after infection, mixed with low-gelling temperature agarose (type VII; Sigma-Aldrich), and layered onto agarose-coated glass slides. Slides were maintained in the dark at 4°C to gel and were submerged in lysis buffer (2.5 M NaCl, 0.1 M EDTA, 10 mM Trizma base, 1% Triton X-100, and 10% DMSO) for at least 1.5 h. After washing with Tris buffer, slides were incubated for 1 h in alkaline electrophoresis buffer (300 mM NaOH and 1 mM EDTA, pH 10) or in neutral electrophoresis buffer (300 mM sodium acetate, 100 mM Tris-HCl, and 1% DMSO, pH 8.3). Slides were then subjected to electrophoresis for ~40 min at 25 V, air dried, neutralized, and stained with 30 μl ethidium bromide (20 μg/ml^{-1}). Mean comet tail moment was scored for 50 cells/slide by using Comet Imager 1.2.10 software (MetaSystems Inc.).

Online supplemental material

Fig. S1 shows the cell cycle distribution of PR-Set7 in U2OS and normal fibroblasts (A) and in the nuclear localization of HA epitope–tagged PR-Set7 in U2OS cells treated for 1 h with proteasome inhibitor MG132 (B). Fig. S2 shows representative DNA combing pictures in shLuc and shPR7 U2OS cells. Fig. S3 shows 53BP1 localization at spontaneous DNA damage foci in shPR7-depleted U2OS cells and quantification of shPR7 U2OS cells displaying 53BP1 foci after ionizing radiation. Fig. S4 shows the impact of PR-Set7 depletion in proliferation rates and H4-K20me status of HeLa cells. Online supplemental material is available at http://www.jcb.org/cgi/content/full/jcb.200706179/DC1.

We thank V. Gire, J.M. Brondello, J. Piette, V. Dulic, and D. Fisher for providing reagents and cell lines; S. Tuduri, C. De Renty, and V. Coulon for technical support with DNA combing experiments; E. Schwob and P. Pasero for helpful discussions; and G. Pawlak, I. Robbins, H. Woodrich, and E. Fabbrizio for critical readings. We thank the Montpellier Réunion Interorganisme Imaging and Institut Fédératif de Recherche 122 DNA combing platforms for their technical assistance.

This work was performed with the institutional support of the Centre National de la Recherche Scientifique and by grants from the Institut National du Cancer and the Association pour la Recherche sur le Cancer to C. Sardet and E. Julien. M. Tardat was supported by a fellowship from the French government.

Submitted: 25 June 2007
Accepted: 27 November 2007

References

Anglana, M., F. Apiou, A. Bensimon, and M. Debatisse. 2003. Dynamics of DNA replication in mammalian somatic cells: nucleotide pool modulates origin choice and interorigin spacing. *Cell*. 114:385–394.

Baus, F., V. Gire, D. Fisher, J. Piette, and V. Dulic. 2003. Permanent cell cycle exit in G2 phase after DNA damage in normal human fibroblasts. *EMBO J.* 22:3992–4002.

Bartkova, J., Z. Horejsi, K. Koed, A. Kramer, F. Tort, K. Zieger, P. Guldberg, M. Sehested, J.M. Nesland, C. Lukas, et al. 2005. DNA damage response as a candidate anti-cancer barrier in early human tumorigenesis. *Nature*. 434:864–870.

Bartkova J., N. Rezaei, M. Liontos, P. Karakaidos, D. Kletsas, N. Issaeva, L.V. Vassiliou, E. Kolettas, K. Niforou, V.C. Zoumpourlis, et al. 2006. Oncogene-induced senescence is part of the tumorigenesis barrier imposed by DNA damage checkpoints. *Nature*. 444:633–637.

Beisel C., A. Imhof, J. Greene, E. Kremmer, and F. Sauer. 2002. Histone methylation by the *Drosophila* epigenetic transcriptional regulator Ash1. *Nature*. 419:857–862.

Benetti, R., S. Gonzalo, I. Jaco, G. Schotta, P. Klatt, T. Jenuwein, and M.A. Blasco. 2007. Suv4-20h deficiency results in telomere elongation and derepression of telomere recombination. *J. Cell Biol.* 178:925–936.

Botuyan, M.V., J. Lee, I.M. Ward, J.E. Kim, J.R. Thompson, J. Chen, and G. Mer. 2006. Structural basis for the methylation state-specific recognition of histone H4-K20 by 53BP1 and Crb2 in DNA repair. *Cell*. 127:1361–1373.

Chuang, L.S., H.I. Ian, T.W. Koh, H.H. Ng, G. Xu, and B.F. Li. 1997. Human DNA-(cytosine-5) methyltransferase-PCNA complex as a target for p21WAF1. *Science*. 277:1996–2000.

Couture, J.F., E. Collazo, J.S. Brunzelle, and R.C. Trievel. 2005. Structural and functional analysis of SET8, a histone H4 Lys-20 methyltransferase. *Genes Dev.* 19:1455–1465.

Cullen, B.R. 2006. Enhancing and confirming the specificity of RNAi experiments. *Nat. Methods*. 3:677–681.

Davey, C.A., D.F. Sargent, K. Luger, A.W. Maeder, and T.J. Richmond. 2002. Solvent mediated interactions in the structure of the nucleosome core particle at 1.9 a resolution. *J. Mol. Biol.* 319:1097–1113.

Delaval, K., J. Govin, F. Cerqueira, S. Rousseaux, S. Khochbin, and R. Feil. 2007. Differential histone modifications mark mouse imprinting control regions during spermatogenesis. *EMBO J.* 26:720–729.

De Nooij, J.C., and I.K. Hariharan. 1995. Uncoupling cell fate determination from patterned cell division in the *Drosophila* eye. *Science*. 270:983–985.

Di Micco, R., M. Fumagalli, A. Cicalese, S. Piccinin, P. Gasparini, C. Luise, C. Schurra, M. Garre, P.G. Nuciforo, A. Bensimon, et al. 2006. Oncogene-induced senescence is a DNA damage response triggered by DNA hyper-replication. *Nature*. 444:638–642.

Doyon, Y., C. Cayrou, M. Ullah, A.J. Landry, V. Cote, W. Selleck, W.S. Lane, S. Tan, X.J. Yang, and J. Cote. 2006. ING tumor suppressor proteins are critical regulators of chromatin acetylation required for genome expression and perpetuation. *Mol. Cell*. 21:51–64.

Duesberg, P., and R. Li. 2003. Multistep carcinogenesis: a chain reaction of aneuploidizations. *Cell Cycle*. 2:202–210.

Esteve, P.O., H.G. Chin, A. Smallwood, G.R. Feehery, O. Gangisetty, A.R. Karpf, M.F. Carey, and S. Pradhan. 2006. Direct interaction between DNMT1 and G9a coordinates DNA and histone methylation during replication. *Genes Dev.* 20:3089–3103.

Fang, J., Q. Feng, C.S. Ketel, H. Wang, R. Cao, L. Xia, H. Erdjument-Bromage, P. Tempst, J.A. Simon, and Y. Zhang. 2002. Purification and functional characterization of SET8, a nucleosomal histone H4-lysine 20-specific methyltransferase. *Curr. Biol.* 12:1086–1099.

Fraga M.F., E. Ballestar, A. Villar-Garea, M. Boix-Chornet, J. Espada, G. Schotta, T. Bonaldi, C. Haydon, S. Ropero, K. Petrie, et al. 2005. Loss of acetylation at Lys16 and trimethylation at Lys20 of histone H4 is a common hallmark of human cancer. *Nat. Genet*. 37:391–400.

Georgi, A.B., P.T. Stukenberg, and M.W. Kirschner. 2002. Timing of events in mitosis. *Curr. Biol.* 12:105–114.

Gorgoulis, V.G., L.V. Vassiliou, P. Karakaidos, P. Zacharatos, A. Kotsinas, T. Liloglou, M. Venere, R.A. Ditullio Jr., N.G. Kastrinakis, B. Levy, et al. 2005. Activation of the DNA damage checkpoint and genomic instability in human precancerous lesions. *Nature*. 434:907–913.

Iizuka, M., T. Matsui, H. Takisawa, and M.M. Smith. 2006. Regulation of replication licensing by acetyltransferase Hbo1. *Mol. Cell. Biol.* 26:1098–1108.

Julien, E., and W. Herr. 2003. Proteolytic processing is necessary to separate and ensure proper cell growth and cytokinesis functions of HCF-1. *EMBO J.* 22:2360–2369.

Julien, E., and W. Herr. 2004. A switch in mitotic histone H4 lysine 20 methylation status is linked to M phase defects upon loss of HCF-1. *Mol. Cell*. 14:713–725.

Karachentsev, D., K. Sarma, D. Reinberg, and R. Steward. 2005. PR-Set7-dependent methylation of histone H4 Lys 20 functions in repression of gene expression and is essential for mitosis. *Genes Dev.* 19:431–435.

Karachentsev, D., M. Druzhinina, and R. Steward. 2007. Free and chromatin-associated mono-, di-, and trimethylation of histone H4-lysine 20 during development and cell cycle progression. *Dev. Biol.* 304:46–52.

Le Cam, L., L.K. Linares, C. Paul, E. Julien, M. Lacroix, E. Hatchi, R. Triboulet, G. Bossis, A. Shmueli, M.S. Rodriguez, et al. 2006. E4F1 is an atypical ubiquitin ligase that modulates p53 effector functions independently of degradation. *Cell*. 127:775–788.

Leonhardt H., A.W. Page, H.U. Weier, and T.H. Bestor. 1992. A targeting sequence directs DNA methyltransferase to sites of DNA replication in mammalian nuclei. *Cell*. 71:865–873.

Mallette, F.A., M.F. Gaumont-Leclerc, and G. Ferbeyre. 2007. The DNA damage signaling pathway is a critical mediator of oncogene-induced senescence. *Genes Dev.* 21:43–48.

Michalet, X., R. Ekong, F. Fougerousse, S. Rousseaux, C. Schurra, N. Hornigold, M. van Slegtenhorst, J. Wolfe, S. Povey, J.S. Beckmann, and A. Bensimon. 1997. Dynamic molecular combing: stretching the whole human genome for high-resolution studies. *Science*. 277:1518–1523.

Murr, R., J.I. Loizou, Y.G. Yang, C. Cuenin, H. Li, Z.Q. Wang, and Z. Herceg. 2006. Histone acetylation by Trrap-Tip60 modulates loading of repair proteins and repair of DNA double-strand breaks. *Nat. Cell Biol.* 8:91–99.

Nishioka, K., J.C. Rice, K. Sarma, H. Erdjument-Bromage, J. Werner, Y. Wang, S. Chuikov, P. Valenzuela, P. Tempst, R. Steward, et al. 2002. PR-Set7 is a nucleosome-specific methyltransferase that modifies lysine 20 of histone H4 and is associated with silent chromatin. *Mol. Cell*. 9:1201–1213.

Nishitani, H., N. Sugimoto, V. Roukos, Y. Nakanishi, M. Saijo, C. Obuse, T. Tsurimoto, K.I. Nakayama, K. Nakayama, M. Fujita, et al. 2006. Two E3 ubiquitin ligases, SCF-Skp2 and DDB1-Cul4, target human Cdt1 for proteolysis. *EMBO J.* 25:1126–1136.

Pasero, P., A. Bensimon, and E. Schwob. 2002. Single-molecule analysis reveals clustering and epigenetic regulation of replication origins at the yeast rDNA locus. *Genes Dev.* 16:2479–2484.

Peters A.H., S. Kubicek, K. Mechtler, R.J. O'Sullivan, A.A. Derijck, L. Perez-Burgos, A. Kohlmaier, S. Opravil, M. Tachibana, Y. Shinkai, J.H. Martens, and T. Jenuwein. 2003. Partitioning and plasticity of repressive histone methylation states in mammalian chromatin. *Mol. Cell.* 12:1577–1589.

Rayasam, G.V., O. Wendling, P.O. Angrand, M. Mark, K. Niederreither, L. Song, T. Lerouge, G.L. Hager, P. Chambon, and R. Losson. 2003. NSD1 is essential for early post-implantation development and has a catalytically active SET domain. *EMBO J.* 22:3153–3163.

Rice, J.C., K. Nishioka, K. Sarma, R. Steward, D. Reinberg, and C.D. Allis. 2002. Mitotic-specific methylation of histone H4 Lys 20 follows increased PR-Set7 expression and its localization to mitotic chromosomes. *Genes Dev.* 16:2225–2230.

Sancar, A., L.A. Lindsey-Boltz, K. Unsal-Kacmaz, and S. Linn. 2004. Molecular mechanisms of mammalian DNA repair and the DNA damage checkpoints. *Annu. Rev. Biochem.* 73:39–85.

Sanders, S.L., M. Portoso, J. Mata, J. Bahler, R.C. Allshire, and T. Kouzarides. 2004. Methylation of histone H4 lysine 20 controls recruitment of Crb2 to sites of DNA damage. *Cell*. 119:603–614.

Sakaguchi, A., and R. Steward. 2007. Aberrant monomethylation of histone H4 lysine 20 activates the DNA damage checkpoint in *Drosophila melanogaster*. *J. Cell Biol.* 176:155–162.

Sarraf, S.A., and I. Stancheva. 2004. Methyl-CpG binding protein MBD1 couples histone H3 methylation at lysine 9 by SETDB1 to DNA replication and chromatin assembly. *Mol. Cell*. 15:595–605.

Scheffner, M., J.M. Huibregtse, R.D. Vierstra, and P.M. Howley. 1993. The HPV-16 E6 and E6-AP complex functions as a ubiquitin-protein ligase in the ubiquitination of p53. *Cell*. 75:495–505.

Schotta, G., M. Lachner, K. Sarma, A. Ebert, R. Sengupta, G. Reuter, D. Reinberg, and T. Jenuwein. 2004. A silencing pathway to induce H3-K9 and H4-K20 trimethylation at constitutive heterochromatin. *Genes Dev.* 18:1251–1262.

Senga, T., U. Sivaprasad, W. Zhu, J.H. Park, E.E. Arias, J.C. Walter, and A. Dutta. 2006. PCNA is a cofactor for Cdt1 degradation by CUL4/DDB1-mediated N-terminal ubiquitination. *J. Biol. Chem.* 281:6246–6252.

Shi, X., I. Kachirskaia, H. Yamaguchi, L.E. West, H. Wen, E.W. Wang, S. Dutta, E. Appella, and O. Gozani. 2007. Modulation of p53 function by SET8-mediated methylation at lysine 382. *Mol. Cell*. 27:636–646.

Sogame, N., M. Kim, and J.M. Abrams. 2003. *Drosophila* p53 preserves genomic stability by regulating cell death. *Proc. Natl. Acad. Sci. USA*. 100:4696–4701.

Taylor, W.R., and G.R. Stark. 2001. Regulation of the G2/M transition by p53. *Oncogene*. 20:1803–1815.

Trojer P., G. Li, R.J. Sims 3rd, A. Vaquero, N. Kalakonda, P. Boccuni, D. Lee, H. Erdjument-Bromage, P. Tempst, S.D. Nimer, Y.H. Wang, and D. Reinberg. 2007. L3MBTL1, a histone-methylation-dependent chromatin lock. *Cell*. 129:915–928.

Venkitaraman, A.R. 2005. Aborting the birth of cancer. *Nature*. 434:829–830.

Xiao, B., C. Jing, G. Kelly, P.A. Walker, F.W. Muskett, T.A. Frenkiel, S.R. Martin, K. Sarma, D. Reinberg, S.J. Gamblin, and J.R. Wilson. 2005. Specificity and mechanism of the histone methyltransferase Pr-Set7. *Genes Dev.* 19:1444–1454.